MOLECULAR IMAGING AND BIOLOGY

Mol Imaging Biol (2019) 21:382–390
DOI: 10.1007/s11307-018-1231-x

Published Online: 9 July 2018

RESEARCH ARTICLE

# How Long of a Dynamic 3′-Deoxy-3′-[$^{18}$F]fluorothymidine ([$^{18}$F]FLT) PET Acquisition Is Needed for Robust Kinetic Analysis in Breast Cancer?

Jun Zhang,[1] Xiaoli Liu,[1] Michelle I. Knopp,[1] Bhuvaneswari Ramaswamy,[2] Michael V. Knopp[1]

[1]*Wright Center of Innovation in Biomedical Imaging, Department of Radiology, The Ohio State University Wexner Medical Center, 395 W. 12th Avenue, Room 430, Columbus, OH, 43210-1228, USA*
[2]*Department of Internal Medicine, The Ohio State University Wexner Medical Center, Columbus, OH, 43210, USA*

**Abstract**

*Purpose:* To quantitatively evaluate the minimally required scanning time of 3′-deoxy-3′-[$^{18}$F]fluorothymidine ([$^{18}$F]FLT) positron emission tomography (PET) dynamic acquisition for accurate kinetic assessment of the proliferation in breast cancer tumors.

*Procedures:* Within a therapeutic intervention trial, 26 breast tumors of 8 breast cancer patients were analyzed from 30-min dynamic [$^{18}$F]FLT-PET acquisitions. PET/CT was acquired on a Gemini TF 64 system (Philips Healthcare) and reconstructed into 26 frames ($8 \times 15$ s, $6 \times 30$ s, $5 \times 1$ min, $5 \times 2$ min, and $2 \times 5$ min). Maximum activity concentrations (Bq/ml) of volume of interests over tumors and plasma in descending aorta were obtained over time frames. Kinetic parameters were estimated using in-house developed software with the two-tissue three-compartment irreversible model (2TCM) ($K_1$, $k_2$, $k_3$, and $K_i$; $k_4 = 0$) and Patlak model ($K_i$) based on different acquisition durations ($T_d$) (10, 12, 14, 16, 20, 25, and 30 min, separately). Different linear regression onset time ($T_0$) points (1, 2, 3, 4, and 5 min) were applied in Patlak analysis. $K_i$ of the 30-min data set was taken as the gold standard for comparison. Pearson product-moment correlation coefficient ($R$) of 0.9 was chosen as a limit for the correlation.

*Results:* The correlation of kinetic parameters between the gold standard and the abbreviated dynamic data series increased with longer $T_d$ from 10 to 30 min. $k_2$ and $k_3$ using 2TCM and $K_i$ using Patlak model revealed poor correlations for dynamic PET with $T_d \leq 14$ min ($k_2$: $R = 0.84$, 0.85, 0.86; $k_3$: $R = 0.67$, 0.67, 0.67; $K_i$: $R = 0.72$, 0.78, 0.87 at $T_d = 10$, 12, and 14 min, respectively). Excellent correlations were shown for all kinetic parameters when $T_d \geq 16$ min regardless of the kinetic model and $T_0$ value ($R > 0.9$).

*Conclusions:* This study indicates that a 16-min dynamic PET acquisition appears to be sufficient to provide accurate [$^{18}$F]FLT kinetics to quantitatively assess the proliferation in breast cancer lesions.

**Key words:** 3′-Deoxy-3′-[$^{18}$F]fluorothymidine ([$^{18}$F]FLT), Kinetic modeling, Dynamic PET, Breast Cancer, Acquisition duration

Jun Zhang and Xiaoli Liu are co-first authors and have contributed equally.

*Correspondence to:* Michael Knopp; *e-mail:* knopp.16@osu.edu

## Introduction

Breast cancer is one of the most common cancers in the USA and the second leading cause of cancer death among women. In 2017, an estimated 252,710 new invasive breast cancer cases and approximately 40,610 women and 460 men breast cancer deaths occurred [1]. Positron emission tomography (PET) as a non-invasive molecular imaging technique has been widely explored with respect to applications in breast cancer diagnosis [2–5]. While 2′-deoxy-2′-[$^{18}$F]-fluoro-D-glucose ([$^{18}$F]FDG) has been used as the main PET tracer in breast cancer to reflect glucose metabolism of breast tumors [2, 6–8], other PET tracers such as [$^{11}$C]methionine as well as [$^{11}$C]thymidine and [$^{18}$F]fluorothymidine ([$^{18}$F]FLT) have also shown clinical potential and values in breast cancer disease detection and therapy response monitoring [6].

[$^{18}$F]FLT-PET gained much attention in the recent years due to its ability to non-invasively quantify cell proliferations in breast cancer and has shown its promising role in breast cancer diagnosis [9–11], breast tumor grading [9], breast tumor heterogeneity visualization [9], early change detection during chemotherapy [12, 13], and long-term therapy response prediction [7, 10, 13]. Comparing to [$^{18}$F]FDG-PET, [$^{18}$F]FLT-PET has better specificity during and after treatment and does not seem to be accumulating in inflammatory processed [14]. It is capable of better differentiating inflammatory tissues from tumors in breast cancer treatment [9] and more predictive of longer-term treatment outcome with early changes [10].

It has been demonstrated that dynamic [$^{18}$F]FLT-PET with kinetic analysis such as tracer influx constant $K_i$ and transport constant $K_1$ is sensitive and robust in assessing and monitoring breast cancer therapy response [7, 10, 12, 13]. Currently reported dynamic [$^{18}$F]FLT-PET acquisitions in breast cancer take about 45 to 95 min, which is time-consuming and uncomfortable which also makes it difficult for clinical routine applications [10, 15]. The long scan time brings challenges in patient comfort and causes related motion artifacts on PET images. The generated bulky data require sophisticated data processing and kinetic analysis.

In this study, a shortened dynamic [$^{18}$F]FLT-PET acquisition protocol was proposed and evaluated through Patlak plot and the two-tissue compartment model kinetic analysis. It aimed to optimize the dynamic [$^{18}$F]FLT-PET in breast cancer with minimum required acquisition time to reduce patient burden and improve system efficiency without compromising imaging quality and quantitative assessment. The established shortened acquisition protocol is to be used as a reference in guiding clinical [$^{18}$F]FLT dynamic PET imaging in breast cancer.

## Materials and Methods

### *Patients*

Twenty-six breast tumor data sets from eight breast cancer patients (age 51.75 ± 11 years, weight 74.33 ± 11.11 kg) were included in this study.

### *Dynamic PET Procedure*

All PET/CT scans were performed using a Gemini TF 64 system (Philips Healthcare). After patient positioning, 30-min dynamic PET scans were initiated immediately after bolus injection of [$^{18}$F]FLT (10.3 ± 0.4 mCi). PET list mode data were reconstructed using 3D row action maximum likelihood algorithm (3D RAMLA) in 26 frames (8 × 15 s, 6 × 30 s, 5 × 1 min, 5 × 2 min, and 2 × 5 min, Fig. 1). Six additional subset dynamic PET data sets were reconstructed and generated using shortened acquisition durations ($T_d$ = 10, 12, 14, 16, 20, and 25 min, separately) (Fig. 1).

### *Image and Data Processing*

All reconstructed images were transferred to the Extended Brilliance Workspace (EBW, Philips Healthcare) for data analysis and evaluation. Spherical volume of interest (VOI) was placed over plasma in the descending aorta well away from the edge (Fig. 2a), and adaptive VOIs by region-grow algorithms were generated to outline breast tumors to obtain

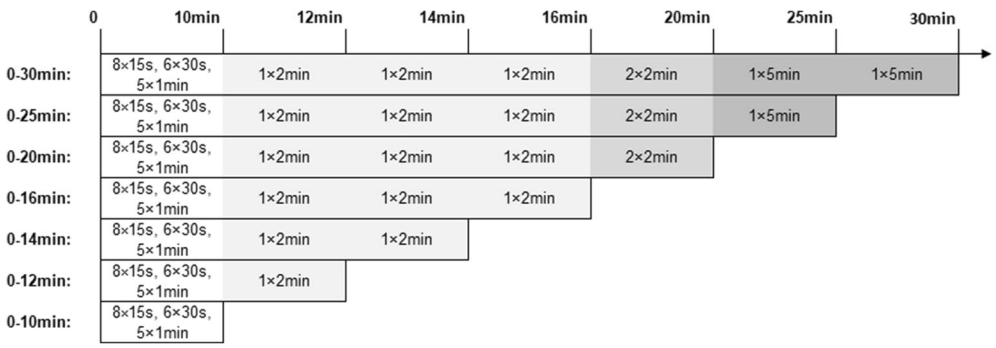


**Fig. 1.** Shortened [$^{18}$F]FLT dynamic PET acquisition durations and time frames used in PET reconstruction as well as kinetic analysis. Thirty-minute acquisition is reduced to shorter acquisitions with the duration of 10, 12, 14, 16, 20, and 25 min.

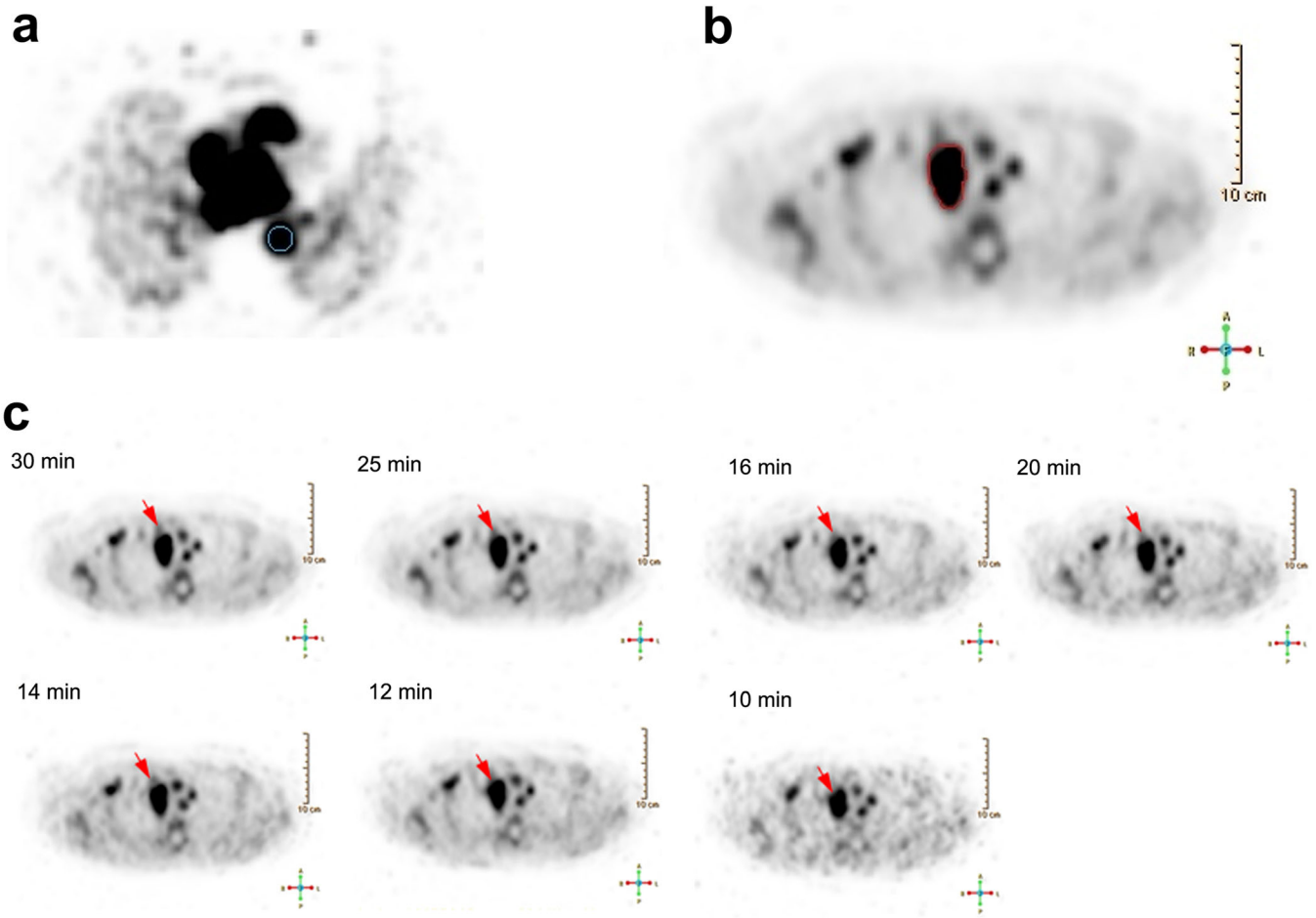


**Fig. 2.** Examples of **a** 3D spherical VOI placement for a plasma uptakes at descending aorta, **b** adaptive VOI contours for tumor uptakes, and **c** tracer uptake of tumors and image quality of dynamic [$^{18}$F]FLT-PET with various acquisition durations (red arrow indicates the location of the target tumor).

the maximum activity concentration (Bq/ml) across all frames (Fig. 2b). Fig. 2c shows an example of PET images under various acquisition durations.

With in-house developed software, kinetic parameters were calculated by both the two-tissue three-compartment irreversible model (2TCM) using the classic iterative Levenberg-Marquardt algorithm and the Patlak model. 2TCM usually consists of plasma, free ligand/non-specific binding in tissue and specific binding, with four rate constants $K_1$–$k_4$ estimated to describe the exchange of the radiotracer between blood and tissue [16]. In the case of [$^{18}$F]FLT, $K_1$ reflects forward transport, $k_2$ the reverse transport, $k_3$ the phosphorylation rate, and $k_4$ the dephosphorylation rate [17]. $k_4$ was set to be zero in this study. The kinetic parameter $K_i$ representing the net influx of radiotracer into the irreversible compartment was obtained using $K_i = K_1 \times k_3/(k_2 + k_3)$ with the plasma input [18]. On the other hand, Patlak model as a graphical analysis model using linear regression to identify the tracer kinetics [19] estimates its key parameter $K_i$ by calculating the slope value of the linear regression. Several onset time points for the Patlak linear regression ($T_0$) were specified in this study to determine the time after which the linear approximation is valid (1, 2, 3, 4, and 5 min, separately). Kinetic parameters estimated from 30-min data sets using 2TCM were taken as the gold standard for comparison.

The mean and maximum SUV values ($SUV_{mean}$ and $SUV_{max}$) with various $T_d$ were collected to assess the quality of the dynamic PET images together with signal-to-noise ratio (SNR) and contrast-to-noise ratio (CNR) which are defined as follows [20]:

$$SNR = \frac{\mathrm{SUVmean}_{\mathrm{liver}}}{SD_{\mathrm{liver}}}$$

$$CNR = \frac{\mathrm{SUVmean}_{\mathrm{tumor}} - \mathrm{SUVmean}_{\mathrm{background}}}{SD_{\mathrm{tumor}}}$$

A circular 2D ROI with the diameter of 50 mm was placed over a normal liver area on the axial image to obtain the $SUV_{mean}$ and SD values. Adaptive 3D VOIs by region-grow were placed for tumors, and spherical 3D VOIs with a diameter of 20 mm were placed on normal breast tissues in a

consistent manner across all dynamic frames. $SUV_{max}$ values were compared between dynamic PET with shortened $T_d$ and the original 30-min acquisition.

### *Statistical Analysis*

Two-tailed *T* test (Microsoft Excel 2016) was applied for the comparisons of SNR, CNR, and SUVs between the values obtained by the shortened data series and those by the 30-min data series. Statistical significance was set at $p < 0.05$ for all tests. Pearson product-moment correlation coefficient ($R$) of 0.9 was chosen as a limit.

## Results

Dynamic [$^{18}$F]FLT-PET images with various acquisition durations were visually evaluated. Twenty-three out of 26 lesions could be clearly defined at $T_d = 10$ min. Only 3 lesions required longer acquisition durations for tumor delineation ($T_d > 16$ min). The average size of the 23 lesions is $21 \pm 11$ mm and $9 \pm 3$ mm for the remaining 3 lesions. Tumor contouring could be easily defined in all images, while the visual quality was apparently improved as the acquisition duration increased (Fig. 2c).

Two quantitative analyses were performed to further evaluate the image quality of the shortened dynamic [$^{18}$F]FLT-PET compared to the 30-min data sets. The first one was conducted by determining SNR (Fig. 3a) and CNR (Fig. 3b). Statistically significant difference was revealed between the 10-min data and the 30-min data with $p = 0.016$ for SNR and $p = 0.008$ for CNR, while no significant difference obtained for the shortened acquisition durations (from 12 to 25 min) compared to the 30-min data (SNR: $p = 0.357$, 0.519, 0.710, 0.493, and 0.686; CNR: $p = 0.098$, 0.073, 0.054, 0.148, and 0.257 at $T_d = 12$, 14, 16, 20, and 25 min, respectively). The second quantitative analysis was performed for $SUV_{max}$ (Fig. 3c) and $SUV_{mean}$ (Fig. 3d). No statistical significance was reached for the comparison based on either $SUV_{max}$ or $SUV_{mean}$ ($SUV_{max}$: $p = 0.373$, 0.337, 0.327, 0.407, 0.577, and 0.679; $SUV_{mean}$: $p = 0.278$, 0.327, 0.265, 0.358, 0.552, and 0.641 at $T_d = 10$, 12, 14, 16, 20, and 25 min, respectively). SUV measurements appeared robust across shortened dynamic [$^{18}$F]FLT-PET acquisitions. Based on these results, shortened acquisition with $T_d \geq 12$ min can

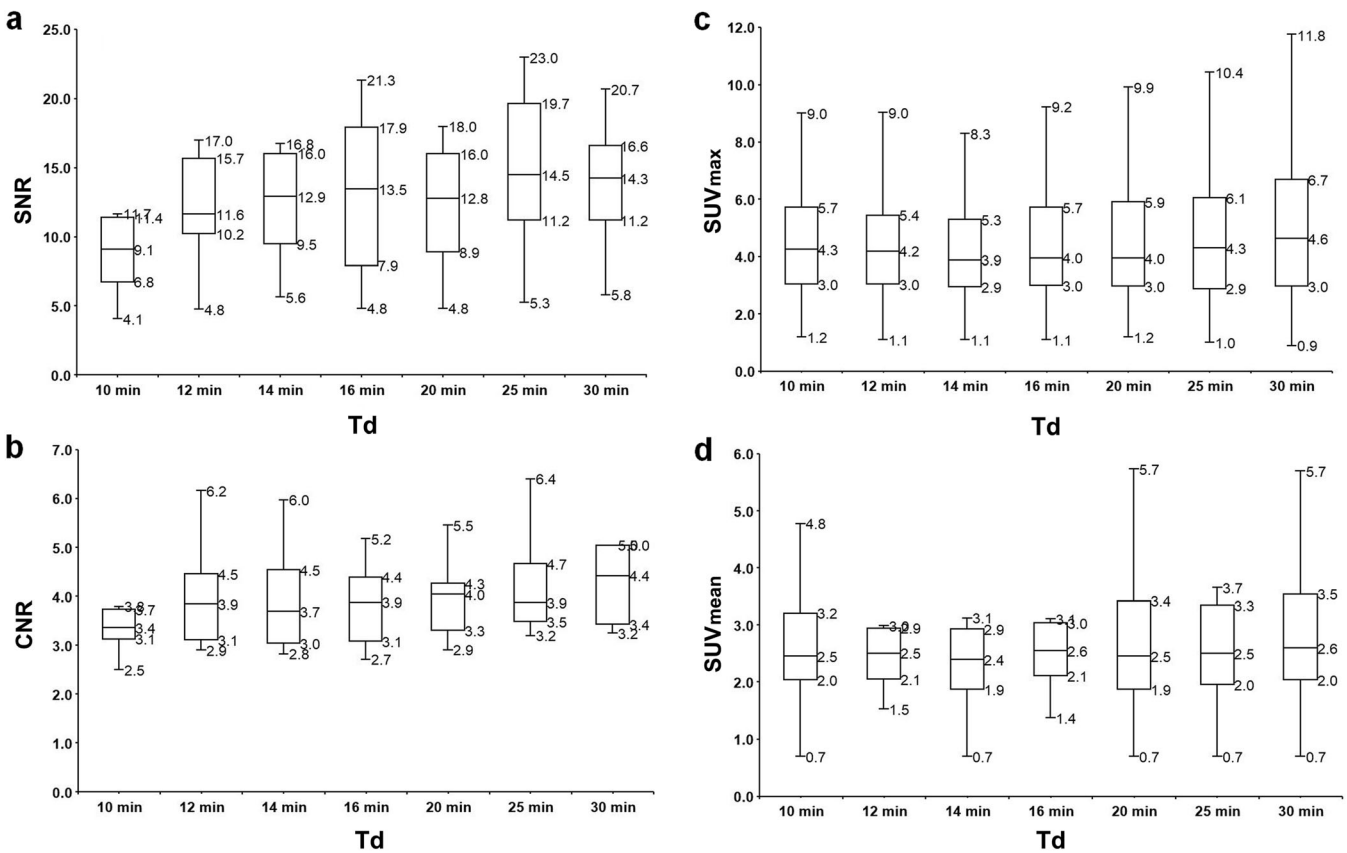


**Fig. 3.** Boxplot of **a** SNR, **b** CNR, **c** $SUV_{max}$, and **d** $SUV_{mean}$ distribution as a function of acquisition duration ($T_d$). Five values (minimum, first quartile, median, third quartile, and maximum in bottom-up order) are summarized. Statistically no significant differences found between the shortened acquisition durations ($T_d = 12$ to 25 min) and the 30-min data for SNR, CNR, and SUV, except $T_d = 10$ min.

provide good quality dynamic images with stable CNR, SNR, and SUV measurements.

Kinetics analysis was performed to verify the quantification accuracy of the kinetic parameters with the shortened acquisitions, as shown in Fig. 4. Using Patlak model, $K_i$ values from all data sets at different onset time ($T_0 = 1$–5 min) are given in Fig. 4a, and the correlations of $K_i$ between shortened and 30-min data sets can be found in Fig. 4b. While the correlation consistently increases with longer acquisition duration, $K_i$ values at $T_d \geq 16$ min presented with high correlations ($R = 0.90$ at $T_d = 16$ min, 0.97 at $T_d = 20$ min, and 1.00 at $T_d = 25$ min), and $K_i$ values at $T_d \leq 14$ min revealed relatively poor correlations ($R < 0.9$). Onset time $T_0$ did not seem to have significant impact on differentiating the excellent and poor correlations of $K_i$ when using the Patlak model. Kinetic parameters ($K_i$, $K_1$, $k_2$, and $k_3$) estimated by 2TCM are shown in Fig. 4c, with corresponding correlations between shortened and 30-min data sets given in Fig. 4d. It demonstrates more consistent measurements of $K_1$, $k_2$, and $k_3$ (in terms of median, first quartile, and third quartile distributions) for $T_d \geq 16$ min than $T_d \leq 14$ min (Fig. 4c). Correlation coefficients of $K_i$ and $K_1$ appeared to be robust and excellent with all shortened acquisitions ($R > 0.9$ for $T_d$ from 10 to 25 min) and increased as increasing the acquisition duration for $k_2$ and $k_3$ (Fig. 4d). $k_2$ and $k_3$ showed excellent correlation when $T_d \geq 16$ min ($k_2$: $R = 0.94$ at $T_d = 16$ min, 0.93 at $T_d = 20$ min, and 1.00 at $T_d = 25$ min; $k_3$: $R = 0.94$ at $T_d = 16$ min, 0.95 at $T_d = 20$ min, and 0.99 at $T_d = 25$ min) and relatively poor correlations when $T_d \leq 14$ min ($k_2$: $R = 0.84$ at $T_d = 10$ min, 0.85 at $T_d = 12$ min, and 0.86 at $T_d = 14$ min; $k_3$: $R = 0.67$ at $T_d = 10$, 12, and 14 min). Based on these results, shortened acquisitions with $T_d \geq 16$ min provide robust measurements of kinetic parameters.

$K_i$ values calculated from Patlak model and 2TCM are compared and shown in Fig. 5. As increasing $T_d$ from 10 to 30 min, the correlation coefficient gradually increased. Excellent correlations were found when $T_d \geq 14$ min ($R = 0.93$ at $T_d = 14$ min, 0.96 at $T_d = 16$ min, 0.98 at $T_d = 20$ min, 0.98 at $T_d = 25$ min, and 0.99 at $T_d = 30$ min), compared to $T_d \leq 12$ min ($R = 0.83$ at $T_d = 10$ min and 0.88 at $T_d = 12$ min). $T_d$ at 14 min could well differentiate the good and poor correlation.

Correlation between $SUV_{max}$ and kinetic parameters ($K_i$, $K_1$, $k_2$, and $k_3$) using 2TCM under $T_d = 10$, 12, 14, 16, 20, 25, and 30 min was additionally evaluated, and the results are shown in Fig. 6. It appeared to be very good correlation

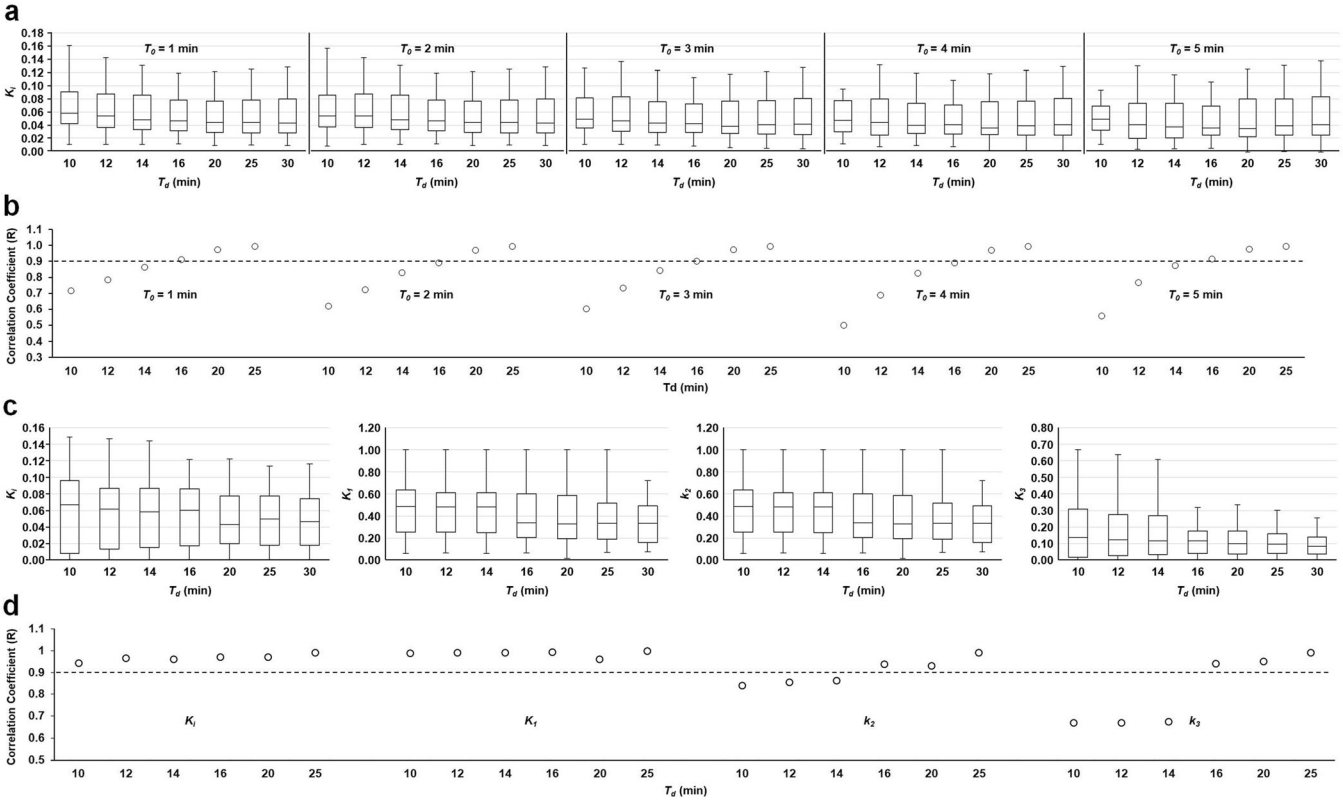


**Fig. 4.** Results of kinetic parameters of [$^{18}$F]FLT dynamic PET with shortened acquisitions compared to 30-min acquisition. **a** Boxplot of Patlak $K_i$ as a function of $T_d$ at onset time points ($T_0$) of 1, 2, 3, 4, and 5 min; **b** correlations of Patlak $K_i$ between shortened and 30-min acquisitions; **c** boxplot of 2TCM kinetic parameters ($K_i$, $K_1$, $k_2$, and $k_3$) as a function of $T_d$; and **d** correlations of 2TCM kinetic parameters between shortened and 30-min dynamic acquisitions. Overall shortened acquisitions with $T_d \geq 16$ min could enable robust estimate of kinetic parameters.

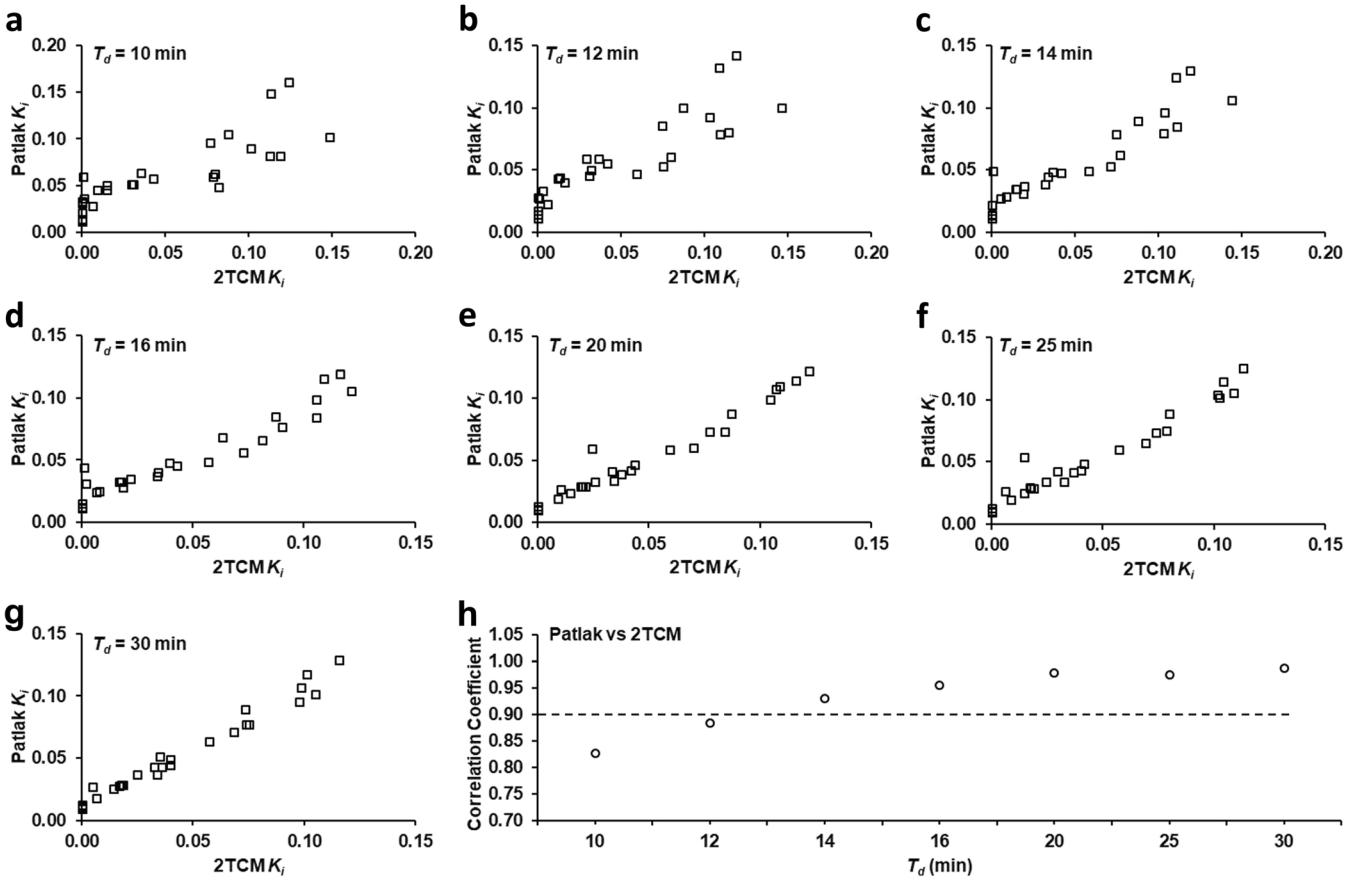


**Fig. 5.** Comparison of calculated $K_i$ values between Patlak and 2TCM methods. **a**–**g** scatterplot of Patlak $K_i$ as a function of 2TCM $K_i$ for each of the 26 breast tumors under [18F]FLT dynamic acquisition durations from 10 to 30 min. **h** Correlation coefficients of $K_i$ estimate from both models as a function of acquisition duration. Excellent correlation ($R \geq 0.90$) was found for shortened acquisition durations at $T_d \geq 14$ min.

between 2TCM $K_i$ and $SUV_{max}$ ($R = 0.87$, 0.89, 0.90, 0.91, 0.93, 0.93, and 0.95), while no strong correlation was found between $SUV_{max}$ and other parameters ($K_1$: $R = 0.63$, 0.61, 0.60, 0.60, 0.56, 0.53, and 0.45; $k_2$: $R = 0.72$, 0.69, 0.68, 0.53, 0.49, 0.39, and 0.27; $k_3$: $R = 0.76$, 0.78, 0.78, 0.75, 0.75, 0.73, and 0.73).

## Discussion

While dynamic [18F]FLT-PET performed on breast cancer patients undergoing chemotherapy has been demonstrated to be helpful in assessing cancer treatment response and predicting the long-term outcome [7, 10, 12, 13], it is challenging to have it implemented in clinical routine applications because of the prolonged scan time. To the best of our knowledge, few studies in breast cancer patients have been published with respect to the use of shortened dynamic PET acquisition. Practically, shortened procedures are requested by patients and patient advocates. Our results showed that compared to 30-min dynamic [18F]FLT-PET imaging, ≥ 12-min dynamic acquisition could provide good quality images for tumor delineation with stable CNR, SNR, and SUV measurements, ≥ 16-min dynamic acquisition could enable robust and accurate [18F]FLT kinetic analysis, and ≥ 14-min dynamic acquisition may lead to well-correlated $K_i$ estimate using different methods (Patlak *vs* 2TCM). Overall, we propose that a 16-min shortened dynamic [18F]FLT-PET acquisition appears to be long enough to facilitate all and will be clinically practicable and feasible from a patient perspective.

Although dynamic [18F]FLT-PET can provide multiple parameters for more detailed tumor response assessment, it is restricted by the limited z-axial field of view of current PET scanners. Specific anatomic regions including the target lesions need to be determined in advance and kept for all follow-up dynamic PET scans. During follow-up examinations and therapy response evaluations, breast cancer metastases as well as recurrent diseases usually occur and need to be detected [21, 22]. Therefore, a modified protocol can be designed with a shortened dynamic [18F]FLT-PET acquisition over the target area and followed by a multiple-bed position static acquisition. The modified protocol may add additional advantages for not only evaluating response of target lesions but also detecting other possible lesions.

Various kinetic models were proposed for quantifying dynamic PET data. The two-tissue compartment model is the

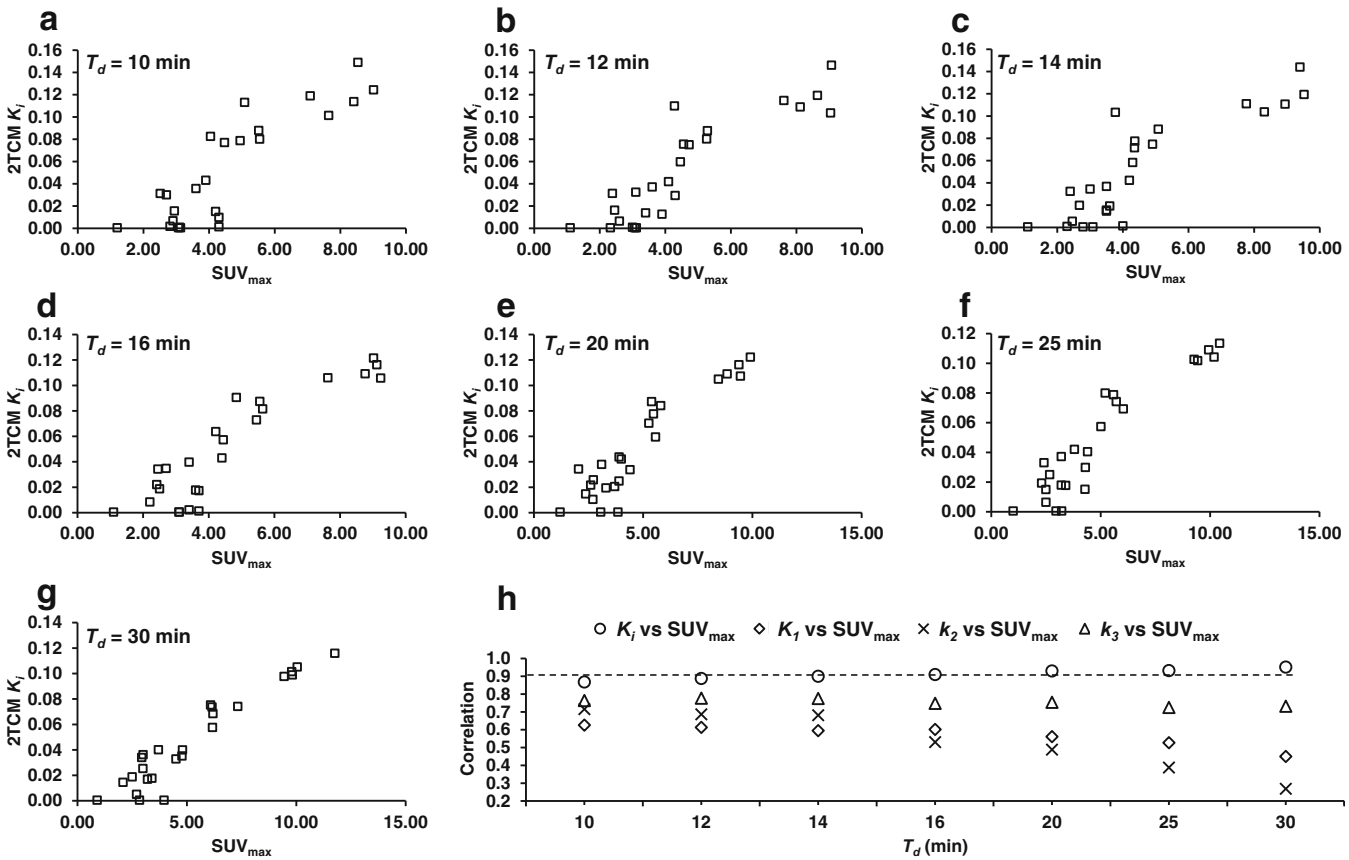


**Fig. 6.** Correlation between $SUV_{max}$ and kinetic parameters ($K_i$, $K_1$, $k_2$, and $k_3$) using 2TCM. **a**–**g** Scatterplot of 2TCM Ki as a function of $SUV_{max}$ at each of the [18F]FLT dynamic acquisition durations. **h** Correlation between 2TCM kinetic parameters and $SUV_{max}$ as a function of acquisition duration. Excellent correlation ($R \geq 0.90$) was found between $K_i$ and $SUV_{max}$ for shortened acquisition durations at $T_d \geq 12$ or 14 min.

most widely applied model in dynamic PET kinetic analysis, while Patlak as a simplified graphical model is gaining its importance in dynamic PET kinetics assessment in recent years [23, 24]. Previous studies have demonstrated that these models could provide valuable kinetic information to evaluate breast cancer treatment response with traditional dynamic PET acquisitions [14, 25–27]. In our study to evaluate the feasibility of reducing the time required for dynamic [18F]FLT-PET scans, it is worth pointing out that we set $k_4 = 0$ for ≤30-min dynamic PET kinetic analysis using 2TCM, while for longer [18F]FLT PET imaging (*e.g.*, 120 min), $k_4$ might be notable [17]. According to our findings, both models gave well-correlated common kinetic parameter $K_i$ particularly for dynamic [18F]FLT-PET acquisition of ≥ 14 min, and as increasing the acquisition duration, changes of $K_i$ distribution appeared to be more obvious using Patlak model than 2TCM.

Patlak linear regression onset time $T_0$ is another essential factor for generating accurate kinetic parameter and therefore was evaluated. $T_0$ determines the slope of the linear regression line and affects $K_i$ estimate. Since dramatic tracer transportation occurs immediately after tracer injection, no steady state can be reached between plasma and the reversible compartments at the very beginning [19]. In order to minimize the impact of prompt tracer transportation, $T_0$ with various onset time points for Patlak linear regression [19, 28–31] were suggested. In our study, onset time points from 1 to 5 min were tested to confirm the impact of different $T_0$ on $K_i$ estimation for the shortened dynamic acquisition. We found that the tested $T_0$ did not affect $K_i$ estimation apparently, and no dramatic tracer transportation was identified 1 to 5 min post [18F]FLT injection. In addition, our data indicated that even a 5–16-min dynamic acquisition ($T_0 = 5$ min) provided accurate $K_i$ estimate. Using the same shortened [18F]FLT dynamic PET data and reconstruction method, 1 min is suggested to be the onset time point for Patlak linear regression in our study. To assure the accuracy, a study with larger data size is required to confirm the findings.

In addition to the dynamic [18F]FLT PET that we explored in this study, [18F]FDG as the most widely used radiotracer is worth testing for clinical applications of implementing shortened dynamic PET acquisition. [18F]FDG displays different uptake patterns in breast tumors

from [18F]FLT according to several clinical studies as well as small animal studies [10, 32]. Within the same breast cancer patient pool or mouse model, [18F]FLT uptake could reach maximal peak or a plateau after approximately 5 to 10 min, compared to that [18F]FDG uptake which gradually increases without reaching a plateau within 60 min post injection. The robustness of the 16-min shortened dynamic [18F]FLT-PET acquisition may be partially contributed by the specific uptake pattern of [18F]FLT. It is possible that the [18F]FLT-based findings in this study may not reflect the truth for [18F]FDG, and a 16-min dynamic acquisition may not be robust for [18F]FDG applications in breast cancer, which needs [18F]FDG-specific evaluation to confirm. In our view, comparison of the performance of multiple radiotracers will also help to establish more robust shortened dynamic PET acquisition protocols.

It is necessary to point out that the metabolite correction for [18F]FLT-PET using two-tissue compartment model was not specifically performed in the evaluation of this pilot study. Researchers found that at 60 min, about 74 % of the blood activity of [18F]FLT was unmetabolized, and a single sample yielded data with mean errors of 2.2 % for metabolite analysis [33]. Ideally, measurement of metabolites in blood is recommended to properly understand more the kinetics of [18F]FLT when evaluating tumor proliferation. This could be added into future studies. This study is limited by the relatively small patient pool, and a larger study with more evaluable tumors and metastases will be necessary to confirm the predictive values.

Lastly, while this study was aiming to investigate whether or not clinical dynamic [18F]FLT PET acquisition could be shortened from the current widely used 45–95-min window [11, 15, 34], we additionally evaluated the correlation between $SUV_{max}$ and kinetic parameters ($K_i$, $K_1$, $k_2$, and $k_3$). In general, SUV as a semi-automatic biomarker can be simply calculated compared to the kinetic parameter determination of dynamic imaging. It would be time-efficient to do a routine static PET only without dynamic PET, if there is a strong correlation between SUV measurements and kinetic parameters. Our data showed that there is a good correlation between $SUV_{max}$ and the $K_i$ parameter under various acquisition durations ($T_d$ = 10–30 min); however, no strong correlation was found between SUV and other kinetic parameters such as $K_1$, $k_2$, and $k_3$. Further, as increasing $T_d$, the correlation between $SUV_{max}$ and $K_1$ as well as between $SUV_{max}$ and $k_2$ becomes less, while the correlation between $SUV_{max}$ and $k_3$ stayed unchanged.

Our study was not powered to answer the question whether an $SUV_{max}$-only assessment is sufficient to provide equivalent conclusions compared kinetic model-based assessment, but instead focus on the impact of acquisition duration. A shorter duration will be more acceptable to patients and thus enable further clinical investigations regarding the most appropriate acquisition approach for this proliferation agent.

## Conclusions

This study indicates that a 16-min dynamic PET acquisition appears to be sufficient to provide accurate [18F]FLT kinetics to quantitatively assess the proliferation in breast cancer lesions. It demonstrates the ability of the shortened [18F]FLT dynamic PET imaging without influencing the kinetic quantification for therapy response assessment, making the use of dynamic acquisitions more clinically feasible.

*Acknowledgements.* The authors acknowledge the help from Preethi Subramanian M.S. for the [18F]FLT data management.

**Funding Information**This project was financially supported by NCI grant U01CA076576, Ohio Third Frontier ODSA TECH09-028, and the Wright Center of Innovation Development Fund.

**Compliance with Ethical Standards**

*Conflict of Interest*

The authors declare that they have no conflict of interest.

## References

1. American Cancer Society. Breast cancer facts & figures 2017–2018 (2017) Atlanta: American Cancer Society, Inc. https://www.cancer.org/content/dam/cancer-org/research/cancer-facts-and-statistics/breast-cancer-facts-and-figures/breast-cancer-facts-and-figures-2017-2018.pdf
2. Escalona S, Blasco JA, Reza MM, Andradas E, Gómez N (2010) A systematic review of FDG-PET in breast cancer. Med Oncol 27:114–129
3. Rosen EL, Eubank WB, Mankoff DA (2007) FDG PET, PET/CT, and breast cancer imaging. Radiographics 27:S215–S229
4. Bensch F, van Kruchten M, Lamberts LE, Schröder CP, Hospers GAP, Brouwers AH, van Vugt MATM, de Vries EGE (2013) Molecular imaging for monitoring treatment response in breast cancer patients. Eur J Pharmacol 717:2–11
5. Oude Munnink TH, Nagengast WB, Brouwers AH et al (2009) Molecular imaging of breast cancer. Breast 18:S66–S73
6. Lavayssiere R, Cabee AE, Filmont JE (2009) Positron emission tomography (PET) and breast cancer in clinical practice. Eur J Radiol 69:50–58
7. Smith IC, Welch AE, Hutcheon AW, Miller ID, Payne S, Chilcott F, Waikar S, Whitaker T, Ah-See AK, Eremin O, Heys SD, Gilbert FJ, Sharp PF (2000) Positron emission tomography using [(18)F]-fluorodeoxy-D-glucose to predict the pathologic response of breast cancer to primary chemotherapy. J Clin Oncol 18:1676–1688
8. Doot RK, Dunnwald LK, Schubert EK, Muzi M, Peterson LM, Kinahan PE, Kurland BF, Mankoff DA (2007) Dynamic and static approaches to quantifying 18F-FDG uptake for measuring cancer response to therapy, including the effect of granulocyte CSF. J Nucl Med 48:920–925
9. Been LB, Suurmeijer AJ, Cobben DC et al (2004) [18F]FLT-PET in oncology: current status and opportunities. Eur J Nucl Med Mol Imaging 31:1659–1672
10. Pio BS, Park CK, Pietras R, Hsueh WA, Satyamurthy N, Pegram MD, Czernin J, Phelps ME, Silverman DHS (2006) Usefulness of 3′-[F-18]fluoro-3′-deoxythymidine with positron emission tomography in predicting breast cancer response to therapy. Mol Imaging Biol 8:36–42
11. Chalkidou A, Landau DB, Odell EW, Cornelius VR, O'Doherty MJ, Marsden PK (2012) Correlation between Ki-67 immunohistochemistry and 18F-Fluorothymidine uptake in patients with cancer: a systematic review and meta-analysis. Eur J Cancer 48:3499–3513

12. Kenny L, Coombes RC, Vigushin DM, al-Nahhas A, Shousha S, Aboagye EO (2007) Imaging early changes in proliferation at 1 week post chemotherapy: a pilot study in breast cancer patients with 3′-deoxy-3′-[18F]fluorothymidine positron emission tomography. Eur J Nucl Med Mol Imaging 34:1339–1347
13. Contractor KB, Kenny LM, Stebbing J, Rosso L, Ahmad R, Jacob J, Challapalli A, Turkheimer F, al-Nahhas A, Sharma R, Coombes RC, Aboagye EO (2011) [18F]-3'Deoxy-3′-fluorothymidine positron emission tomography and breast cancer response to docetaxel. Clin Cancer Res 17:7664–7672
14. Bollineni VR, Kramer GM, Jansma EP, Liu Y, Oyen WJG (2016) A systematic review on [18F]FLT-PET uptake as a measure of treatment response in cancer patients. Eur J Cancer 55:81–97
15. Kenny LM, Vigushin DM, Al-Nahhas A et al (2005) Quantification of cellular proliferation in tumor and normal tissues of patients with breast cancer by [18F]fluorothymidine-positron emission tomography imaging: evaluation of analytical methods. Cancer Res 65:10104–10112
16. Watabe H, Ikoma Y, Kimura Y, Naganawa M, Shidahara M (2006) PET kinetic analysis—compartmental model. Ann Nucl Med 20:583–588
17. Muzi M, Vesselle H, Grierson JR, Mankoff DA, Schmidt RA, Peterson L, Wells JM, Krohn KA (2005) Kinetic analysis of 3′-deoxy-3′-fluorothymidine PET studies: validation studies in patients with lung cancer. J Nucl Med 46:274–282
18. Dimitrakopoulou-Strauss A, Pan L, Strauss LG (2012) Quantitative approaches of dynamic FDG-PET and PET/CT studies (dPET/CT) for the evaluation of oncological patients. Cancer Imaging 12:283–289
19. Patlak CS, Blasberg RG, Fenstermacher JD (1983) Graphical evaluation of blood-to-brain transfer constants from multiple-time uptake data. J Cereb Blood Flow Metab 3:1–7
20. Gramer BM, Muenzel D, Leber V, von Thaden AK, Feussner H, Schneider A, Vembar M, Soni N, Rummeny EJ, Huber AM (2012) Impact of iterative reconstruction on CNR and SNR in dynamic myocardial perfusion imaging in an animal model. Eur Radiol 22:2654–2661
21. Gaeta CM, Vercher-Conejero JL, Sher AC, Kohan A, Rubbert C, Avril N (2013) Recurrent and metastatic breast cancer PET, PET/CT, PET/MRI: FDG and new biomarkers. Q J Nucl Med Mol Imaging 57:352–366
22. Manohar K, Mittal BR, Senthil R, Kashyap R, Bhattacharya A, Singh G (2012) Clinical utility of F-18 FDG PET/CT in recurrent breast carcinoma. Nucl Med Commun 33:591–596
23. Raijmakers P, Temmerman OPP, Saridin CP, Heyligers IC, Becking AG, van Lingen A, Lammertsma AA (2014) Quantification of 18F-fluoride kinetics: evaluation of simplified methods. J Nucl Med 55:1122–1127
24. Veronese M, Rizzo G, Aboagye EO, Bertoldo A (2014) Parametric imaging of F-fluoro-3-deoxy-3-L-fluorothymidine PET data to investigate tumour heterogeneity. Eur J Nucl Med Mol Imaging 41:1781–1792
25. Krak NC, van der Hoeven JJ, Hoekstra OS et al (2003) Measuring [(18)F]FDG uptake in breast cancer during chemotherapy: comparison of analytical methods. Eur J Nucl Med Mol Imaging 30:674–681
26. Dunnwald LK, Gralow JR, Ellis GK, Livingston RB, Linden HM, Specht JM, Doot RK, Lawton TJ, Barlow WE, Kurland BF, Schubert EK, Mankoff DA (2008) Tumor metabolism and blood flow changes by positron emission tomography: relation to survival in patients treated with neoadjuvant chemotherapy for locally advanced breast cancer. J Clin Oncol 26:4449–4457
27. Dunnwald LK, Doot RK, Specht JM, Gralow JR, Ellis GK, Livingston RB, Linden HM, Gadi VK, Kurland BF, Schubert EK, Muzi M, Mankoff DA (2011) PET tumor metabolism in locally advanced breast cancer patients undergoing neoadjuvant chemotherapy: value of static versus kinetic measures of fluorodeoxyglucose uptake. Clin Cancer Res 17:2400–2409
28. Visser EP, Philippens ME, Kienhorst L et al (2008) Comparison of tumor volumes derived from glucose metabolic rate maps and SUV maps in dynamic 18F-FDG PET. J Nucl Med 49:892–898
29. Freedman NM, Sundaram SK, Kurdziel K, Carrasquillo J, Whatley M, Carson J, Sellers D, Libutti S, Yang J, Bacharach S (2003) Comparison of SUV and Patlak slope for monitoring of cancer therapy using serial PET scans. Eur J Nucl Med Mol Imaging 30:46–53
30. Cheebsumon P, Velasquez LM, Hoekstra CJ, Hayes W, Kloet RW, Hoetjes NJ, Smit EF, Hoekstra OS, Lammertsma AA, Boellaard R (2011) Measuring response to therapy using FDG PET: semi-quantitative and full kinetic analysis. Eur J Nucl Med Mol Imaging 38:832–842
31. Mankoff DA, Dunnwald LK, Gralow JR, Ellis GK, Charlop A, Lawton TJ, Schubert EK, Tseng J, Livingston RB (2002) Blood flow and metabolism in locally advanced breast cancer: relationship to response to therapy. J Nucl Med 43:500–509
32. Desilva A, Wuest M, Wang M, Hummel J, Mossman K, Wuest F, Hitt MM (2012) Comparative functional evaluation of immunocompetent mouse breast cancer models established from PyMT-tumors using small animal PET with [18F]FDG and [18F]FLT. Am J Nucl Med Mol Imaging 2:88–98
33. Shields AF, Briston DA, Chandupatla S, Douglas KA, Lawhorn-Crews J, Collins JM, Mangner TJ, Heilbrun LK, Muzik O (2005) A simplified analysis of [18F]3′-deoxy-3′-fluorothymidine metabolism and retention. Eur J Nucl Med Mol Imaging 32:1269–1275
34. Kramer GM, Frings V, Heijtel D, Smit EF, Hoekstra OS, Boellaard R, QuIC-ConCePT Consortium (2017) Parametric method performance for dynamic 3′-deoxy-3'-18F-fluorothymidine PET/CT in epidermal growth factor receptor-mutated non-small cell lung carcinoma patients before and during therapy. J Nucl Med 58:920–925